Research Article

# Computer-assisted analysis of filopod formation and the role of myosin II heavy chain phosphorylation in *Dictyostelium*

**Paul J. Heid, Jeremy Geiger, Deborah Wessels, Edward Voss and David R. Soll***

W.M. Keck Dynamic Image Analysis Facility, Department of Biological Sciences, The University of Iowa, Iowa City, IA 52242, USA

*Author for correspondence (e-mail: david-soll@uiowa.edu)

Journal of Cell Science

## Summary

To investigate the role played by filopodia in the motility and chemotaxis of amoeboid cells, a computer-assisted 3D reconstruction and motion analysis system, DIAS 4.0, has been developed. Reconstruction at short time intervals of *Dictyostelium* amoebae migrating in buffer or in response to chemotactic signals, revealed that the great majority of filopodia form on pseudopodia, not on the cell body; that filopodia on the cell body originate primarily on pseudopodia and relocate; and that filopodia on the uropod are longer and more stable than those located on other portions of the cell. When adjusting direction through lateral pseudopod formation in a spatial gradient of chemoattractant, the temporal and spatial dynamics of lateral pseudopodia suggest that filopodia may be involved in stabilizing pseudopodia on the substratum while the decision is being made by a cell either to turn into a pseudopodium formed in the correct direction (up the gradient) or to retract a pseudopodium formed in the wrong direction (down the gradient). Experiments in which amoebae were treated with high concentrations of chemoattractant further revealed that receptor occupancy plays a role both in filopod formation and retraction. As phosphorylation-dephosphorylation of myosin II heavy chain (MHC) plays a role in lateral pseudopod formation, turning and chemotaxis, the temporal and spatial dynamics of filopod formation were analyzed in MHC phosphorylation mutants. These studies revealed that MHC phosphorylation-dephosphorylation plays a role in the regulation of filopod formation during cell migration in buffer and during chemotaxis. The computer-assisted technology described here for reconstructing filopodia at short time intervals in living cells, therefore provides a new tool for investigating the role filopodia play in the motility and chemotaxis of amoeboid cells.

Key words: 3D-DIAS reconstruction, Cell migration, Filopodia, Myosin II heavy chain phosphorylation, *Dictyostelium discoideum*

## Introduction

Animal cells extend membrane-bound spikes and thread-like structures from their surface, which are referred to as filopodia. These structures form on motile cells in vitro and in vivo, and can be less than 0.1 μm in diameter and up to several cell diameters in length (Johnston et al., 1979; Rifkin and Isik, 1984; Han et al., 2002; Salas-Vidal and Lameli, 2004; De Joussineau et al., 2003; Sato et al., 2003). Like pseudopodia (and lamellipodia), filopodia are highly enriched in F-actin (Small, 1988; Lewis and Bridgeman, 1992). They differ from pseudopodia, however, in F-actin organization. In pseudopodia, F-actin is organized into a complex, crosslinked network that expands through branching and filament growth (Hartwig and Shevlin, 1986; Cox et al., 1995; Svitkina and Borisy, 1999). In filopodia, F-actin is organized into a bundle of unbranched filaments, aligned along the filopod axis (Lewis and Bridgeman, 1992; Small et al., 2002; Svitkina and Borisy, 1999). Labeling experiments have revealed that growth of F-actin in filopodia occurs distally at the barbed end (Mallavarapu and Mitcheson, 1999), supporting a treadmill model (Small, 1994). Recently, it was demonstrated (Svitkina

et al., 2003) that filopodia form through reorganization of the pre-existing cortical F-actin network. A number of proteins have been found to be localized or enriched in filopodia, including myosin I (Tokuo and Ikebe, 2004) and the Ena/VASP proteins (Bear et al., 2002; Han et al., 2002), the latter appearing to inhibit F-actin capping and thus facilitate filament elongation (Mejillano et al., 2004). Although filopodia were described close to a century ago (Clark, 1912), their regulation, function(s) and possible diversity in amoeboid cells responding to extracellular signals are still poorly understood.

To study the role filopodia play in locomotion and chemotaxis, we developed a computer-assisted dynamic image analysis system, DIAS 4.0, which provides 3D reconstructions of the cell surface, nucleus, pseudopodia and filopodia of migrating cells at 4-second intervals. Using this new technology, we analyzed the formation of filopodia by *Dictyostelium* amoebae migrating in buffer, moving in a directed fashion up a spatial gradient of chemoattractant towards an aggregation stream and responding to the rapid addition of chemoattractant (Soll et al., 2002). Through mutant analysis, we then tested whether myosin II heavy chain (MHC) phosphorylation-dephosphorylation plays a role in filopod

formation, as it had been demonstrated to play a role in cell locomotion, responsiveness to chemotactic signals and, most importantly, pseudopod formation (Stites et al., 1998; Heid et al., 2004). The three mutant cell lines were *HS1*, an MHC-null mutant (Manstein et al., 1989), 3XALA, in which the three threonine phosphorylation sites of MHC are replaced with alanine so that it mimics the constitutively unphosphorylated state (Egelhoff et al., 1993; Egelhoff et al., 1996), and 3XASP, in which the three threonine phosphorylation sites of MHC are replaced with aspartate residues so that it mimics the constitutively phosphorylated state (Egelhoff et al., 1993). Our results provide insights into the origin, stability, dynamics and possible function of filopodia, demonstrate that receptor occupancy regulates filopod formation and retraction, and indicate that MHC phosphorylation-dephosphorylation plays a role in the regulation of filopod formation.

## Materials and Methods

### Cell lines and culture conditions

The normal cell line used to analyze the dynamics of filopod formation was JH10. An *mhc* null mutant, HS1, was generated from JH10 by targeted gene replacement (Manstein et al., 1989). JH10, therefore, served as a control for HS1. The wild-type *mhcA* rescue of HS1, HS1-rescue, was generated by transforming HS1 with an autonomously replicating vector containing wild-type *mhcA* regulated by the actin 15 promoter (Egelhoff et al., 1993). 3XASP and 3XALA were generated in a manner similar to HS1-rescue, but in the former mutant the three threonines in the *mhcA* coding region were mutated to aspartate residues and in the latter mutant to alanine residues (Egelhoff et al., 1993). The HS1-rescue, therefore, served as a control for 3XASP and 3XALA.

For experimental purposes, JH10 cells were grown in liquid HL-5 medium (Cocucci and Sussman, 1970) supplemented with 100 µg/ml thymidine. All other strains were grown first in HL-5 medium plus 10 µg/ml G418 for selection and then in HL-5 medium lacking the drug for experimental purposes. Cells were harvested from plates at the confluent monolayer stage, washed with buffered salts solution (Sussman, 1987) and distributed on filter pads saturated with buffered salts solution, as previously described (Heid et al., 2004). Cells were then washed from pads with buffered salts solution at the ripple stage, which represents the onset of aggregation (Soll, 1979) and the time at which mutant and wild-type cells achieved maximum velocity (Varnum et al., 1986; Heid et al., 2004). For analysis in buffer in the absence of chemoattractant, cells were distributed on the glass wall of a Sykes-Moore perfusion chamber (Bellco Glass, Vineland, NJ). After 5 minutes of incubation, the chamber was perfused with buffered salts solution at a rate that turned over one equivalent chamber volume every 15 seconds (Falk et al., 2003; Wessels et al., 1989; Zhang et al., 2002). Perfusion ensured that cells did not condition their microenvironment with the chemoattractant cAMP. A modification of a previously described aggregation chamber (Wessels et al., 1992) was used for the analysis of cells in response to a gradient of chemoattractant released from an aggregation stream. In brief, a hole 17.5 mm in diameter was drilled through the top of a 35 mm plastic Petri dish. The hole was then covered with plastic wrap and sealed with a ring of petroleum jelly followed by a ring of glue. The plastic wrap provided a clear surface suitable for short working distance imaging with high resolution DIC optics. An aliquot of $1.4 \times 10^6$ cells in 0.5 ml BSS was deposited on the plastic wrap and incubated for 30 minutes to allow adherence. An aliquot of 1.5 ml buffered salts solution was then added to the chamber to prevent dehydration during image capture. For responses to the rapid addition of $10^{-6}$ M cAMP, cells were distributed on the wall of a Dvorak-Stotler chamber (Lucas-Highland, Chantilly, VA) and perfused with buffer alone for 5 minutes. Perfusion solution was then switched to buffer containing $10^{-6}$ M cAMP, as previously described (Wessels et al., 1989).

### 3D reconstruction

Cells were imaged through a $63\times$ oil immersion objective (NA 1.4) of a Zeiss ICM405 inverted microscope equipped with DIC optics. The shaft of the focusing knob was attached to an Empire Magnetics (Rohret, CA) IN-23P stepping motor. A Burst Electronics (Corrales, NM) MCG-2 micro character generator was inserted into the video path of a Hitachi KP-M3AN CCD camera to provide synchronization (up/down/pause) information corresponding to motor position. Both motor and character generator were controlled by a customized program written in Linux on a dedicated Intel platform. Only the up-scans were used for reconstructing cells. 60 sections were obtained through the *z*-axis, beginning at the substratum, in a 2-second period. The distance between sections was 0.33 µm, and the total distance for the set of sections 20 µm. The time it took to return to the substratum was 2 seconds. The sectioning process was repeated every 4 seconds. A Sony DV-G1000 digital video recorder was used to convert the live analog camera signal to digital video captured directly onto an iMac using iMovie. The iMovie capture screen allowed the experimenter to adjust the quality of the image and lighting via direct feedback. 1 hour of recording required approximately 15 GB of hard disk space. A customized program then converted the iMovie video to a QuickTime movie, which in turn was connected to a DIAS 4.0 movie (Soll, 1995; Soll and Voss, 1998; Soll et al., 2000; Heid et al., 2002), retaining only the required up-scans. The resulting movies were transferred through a 100 base-T network to a high-performance Windows XP machine equipped with a 3.2 GHz Pentium 4 processor for DIAS reconstruction. Video compression was avoided because of the very fine nature of the filopodia. DIAS 4.0, the successor to the Macintosh-based 3D-DIAS program (Soll, 1995; Soll and Voss, 1998; Soll et al., 2000), was used for dynamic 3D reconstruction. DIAS 4.0 is written in the Java programming language allowing multi-platform support, automatic memory management and the powerful 'Swing' graphical user interface. Sun Microsystems JVM 1.4 and IBM WebSphere implementations of the Java virtual machine provided the necessary speed. The Java interface allowed 'drag-and-drop', 'on-the-fly' processing by simply dragging a movie into a 'processing station'. As the diameters of filopodia were less than 0.1 µm, and because of their length and complex 3D trajectory, automated outlining did not accurately trace filopodia. Therefore, the cell surface, filpodia and cell compartments (nucleus, pseudopodia) were manually outlined with DIAS software. The in-focus edge of the cell body containing particulate cytoplasm, the regions of the cell containing non-particulate cytoplasm (pseudopodial regions), the nucleus, filopodia emanating from the general cell body and pseudopodia, and filopodia (tail fibers) emanating from the uropod, were color-coded green, blue, purple, red and yellow, respectively. The first 12 outlined optical sections through 3.67 µm in the *z*-axis of a representative cell under reconstruction are presented in Fig. 1A. The traces of cell body (green), pseudopodia (blue) and nucleus (red) in each optical section were placed in individual 'trace slots'. The cell body, pseudopodia and nucleus were traced as closed curves (Fig. 1A). Each closed outline was converted to a beta-spline representation (Barsky, 1988) and the result cleaned of spurious pixels. Filopodia, on the other hand, were traced as a series of short line segments in each optical section (Fig. 1A). Outlines of in-focus filopodial line segments are noted with arrows in select optical sections in Fig. 1A. Dilation was used to thicken the filopodial segments to achieve continuity and erosion was used to restore the outline to a more realistic width. Filopodia formed in pseudopodia and the general cell body, other than the uropod, were color-coded red, whereas filopodia from the uropod ('tail fibers') were color-coded yellow.

To generate faceted 3D reconstructions, the beta-spline

**Fig. 1.** The computer-assisted DIAS 4.0 software program provides 3D reconstructions of living cells that include color-coded representations of the general cell body, nucleus, pseudopodia and filopodia. (A) The in-focus edges of cell compartments and filopodia are outlined in each of 60 optical sections beginning at the substratum and ending 20 μm above the substratum. Cells are imaged by differential interference contrast (DIC) microscopy. The set of 60 optical sections is collected in a 2-second period and the procedure repeated at intervals of 4 seconds. The outline of the in-focus cell body containing particulate cytoplasm is color-coded green, outlines of the in-focus pseudopodial protrusions containing non-particulate cytoplasm are color-coded blue, the outline of the nucleus is color-coded fuchsia, filopodial segments emanating from the general cell body and pseudopodia are color-coded red and filopodia emanating from the uropod, referred to here as tail fibers, are color-coded yellow. Only the first 12 outlined optical sections, beginning at the substratum (0 μm) are presented here, of a cell turning towards an aggregation stream in response to a gradient of chemoattractant late in the *Dictyostelium* aggregation process. (B) Reconstruction of the outlined cell viewed at 10°, 30° and 55° from three rotational vantage points. The arrows in each rotation illustrated at the top of the panels reflect the posterior-anterior axis deduced from the prior history of cellular translocation. The capacity to view the cell from different angles provides a more complete picture of filopod location and interaction with the substratum. The cell body is a transparent mesh and color-coded green, the nucleus is color-coded fuchsia, the pseudopodial regions are color-coded gray, the filopodia are color-coded red and the tail fibers emanating from the uropod are color-coded yellow. Bar, 5 μm.
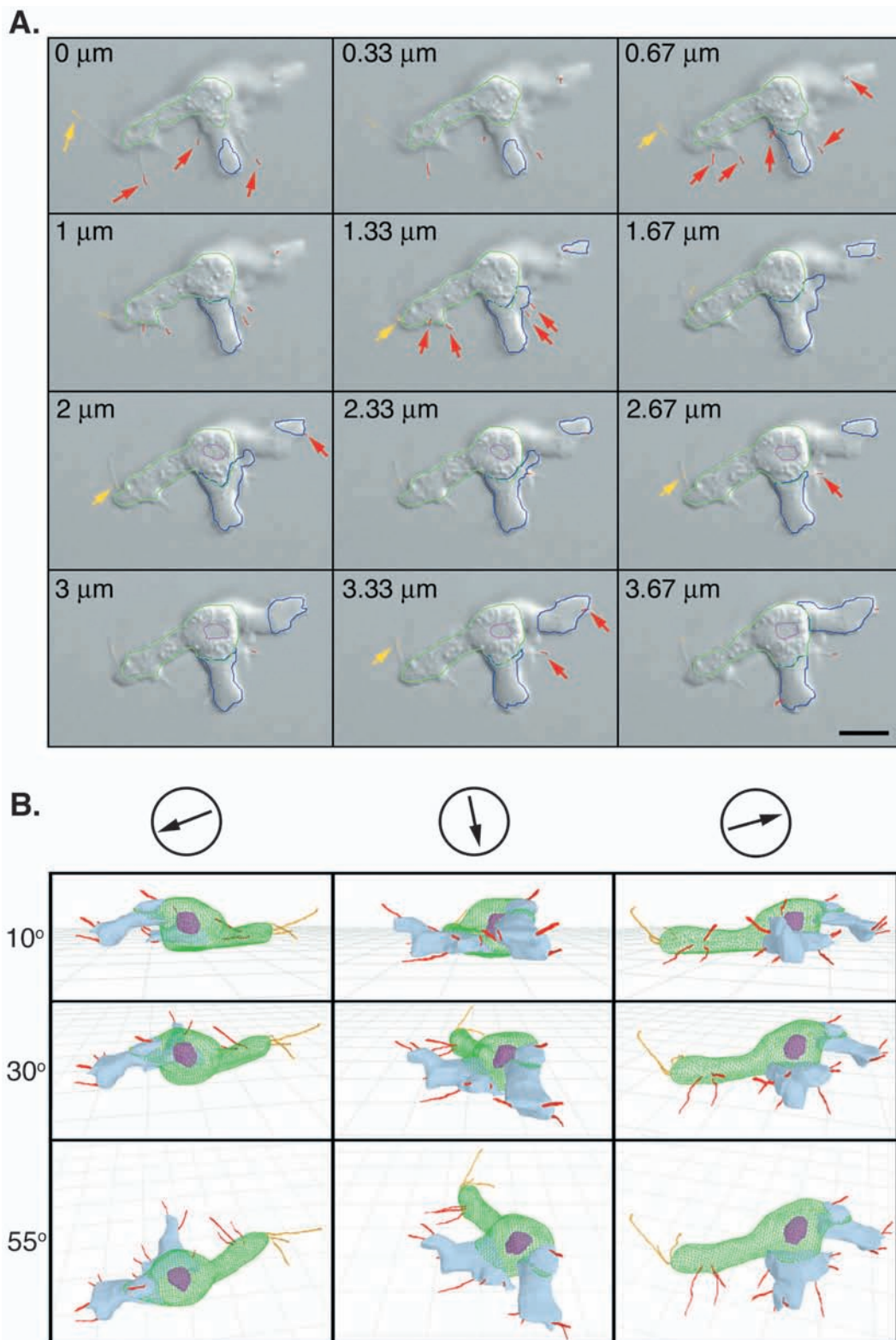
representations of the closed outlines representing cell body, pseudopodia and nucleus were stacked and processed according to methods previously described (Soll et al., 2000). The original DIAS program was extended from the original limit of 7000 facets per object to 200,000 facets per object, by rewriting the original C-code of 3D-DIAS into Java, using object-oriented techniques and native memory management. To render a high-quality 3D image containing up to 500,000 facets, hardware rendering was required. An NVIDIA GeForce Ti4200 video display board was used for this purpose. To communicate with the board, the OpenGL (Silicon Graphics) 3D
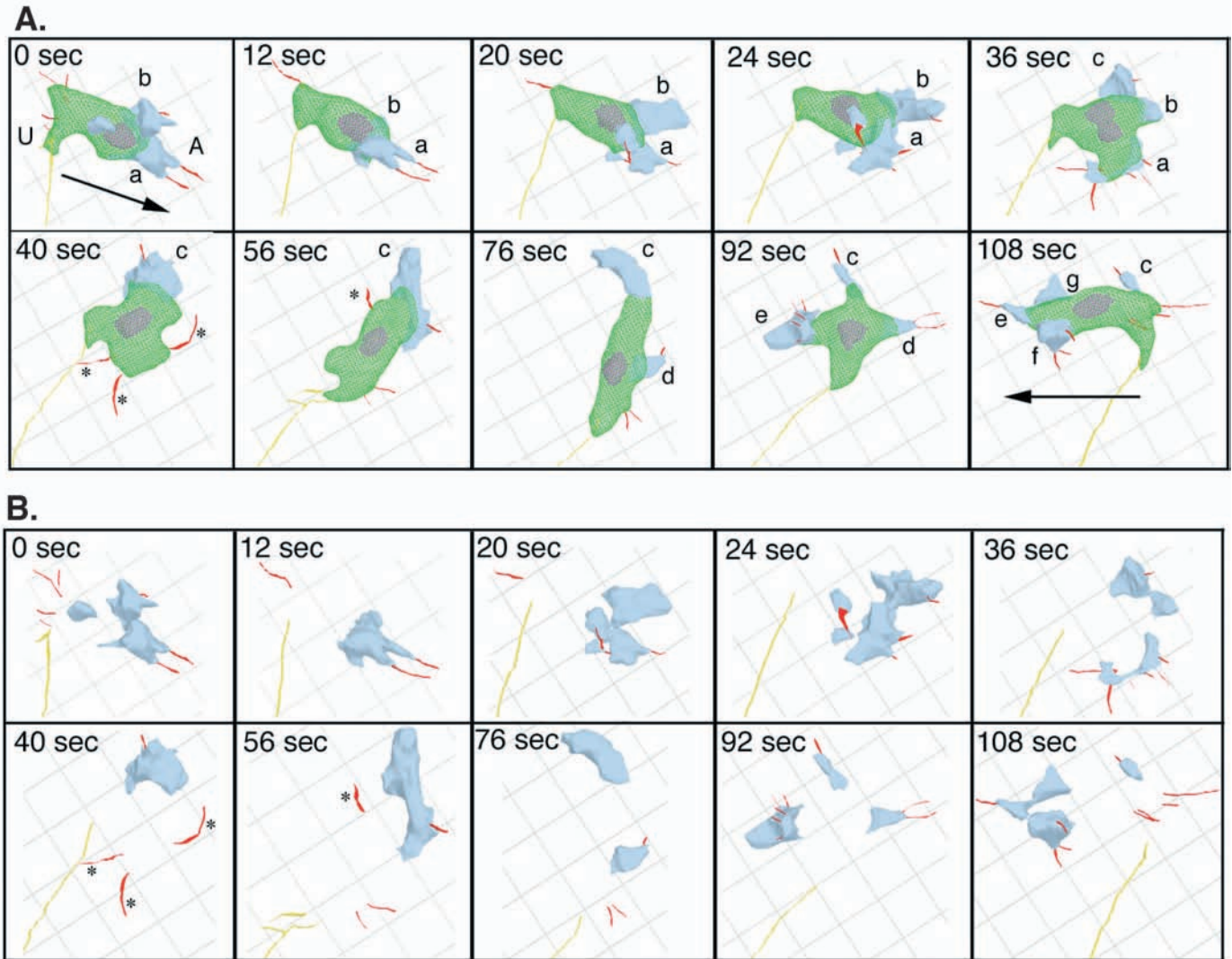
**Fig. 2.** Filopod formation, retraction and relocation for a representative cell migrating in buffer. (A) Reconstruction of the full cell, including nucleus, pseudopodia and filopodia. (B) Reconstruction only of pseudopodia and filopodia. The cell is viewed from the top (90°). Time is presented in seconds (sec). The arrows at 0 and 108 seconds in panel A reflect changes in orientation of the posterior-anterior axis during the time of analysis. See legend to Fig. 1B for color code. A, anterior end of cell; U, uropod; a, b, c, d, e, f, g, pseudopods in order of appearance. Note that the long yellow tail fiber is much longer than shown, and is truncated by the area of view and that the uropod and long tail fiber are stable throughout the period of analysis. Note also that the starred filopodia on the cell body in panel A, 40 sec, originated on pseudopod a and that the starred filopod on the cell body in panel A, 56 sec, originated on pseudopod c.

graphics language was used. GL4Java (Jausoft, Hildesheim, Germany) Open GL libraries were used to connect DIAS 4.0 to the hardware. DIAS controlled the lighting, color, texture, size and view angle of the image through multiple control panels in a GL reconstruction processing station. For smoothing, the $x$, $y$ and $z$ coordinates of each vertex were averaged with the coordinates of directly adjacent vertices, using equal weights. Usually three rounds of such smoothing were applied. In Fig. 1B, the final 3D reconstruction of the cell outlined in Fig. 1A is viewed from three angles (10°, 30°, 55°) each at three rotational vantage points to facilitate analyses of filopod origin and relocation.

## Results

### Filopod formation, retraction and relocation in buffer

*Dictyostelium* amoebae migrating in buffer in the absence of chemoattractant were polar, with a definable dominant anterior pseudopod, one or more lateral pseudopods and a posterior uropod (Fig. 2A, 0 second). These cells possessed on average $5.1\pm1.6$ ($n=24$) filopodia per cell. The range was three to eight per cell. In Fig. 2B, the cell body has been subtracted from each reconstruction, leaving only pseudopodia and filopodia, in order to obtain a better view of the relationships between filopodia and pseudopodia. At 0 seconds, the cell possessed a dominant anterior pseudopod (a) and a closely positioned lateral pseudopod (b). Two filopodia emanated from pseudopod a, one from pseudopod b, three from the cell body and one branched filopod from the uropod (Fig. 2A,B). Between 0 and 24 seconds, pseudopod a expanded to the right of the cell, causing the cell to rotate in a clockwise direction (Fig. 2A). Between 24 and 40 seconds, both pseudopod a and

**Table 1. Mapping the origin of filpodia (including tail fibers) over time for a cell migrating in buffer and a cell migrating towards an aggregation stream**

Migration in buffer (cell in Fig. 2)

| Cell location | Number of filopodia at each time point (seconds) | | | | | | | | | |
|---|---|---|---|---|---|---|---|---|---|---|
| | 0 | 12 | 20 | 24 | 36 | 40 | 56 | 76 | 92 | 108 |
| Pseudopodium a | 2 | 2 | 3 | 3 | 6 | – | – | – | – | – |
| Pseudopodium b | 1 | 0 | 0 | 1 | 0 | – | – | – | – | – |
| Pseudopodium c | – | – | – | – | 1 | 1 | 1 | 0 | 1 | 1 |
| Pseudopodium d | – | – | – | – | – | – | – | 1 | 2 | – |
| Pseudopodium e | – | – | – | – | – | – | – | – | 5 | 1 |
| Pseudopodium f | – | – | – | – | – | – | – | – | – | 3 |
| Cell body[a] | 4 | 1 | 1 | 1[a] | 0 | 3[a] | 2[a],1[c] | 2[a] | 0 | 2, 2[d] |
| Uropod | 2 | 1 | 1 | 1 | 1 | 1 | 2 | 1 | 1 | 1 |
| Total | 9 | 4 | 5 | 6 | 8 | 5 | 6 | 4 | 9 | 10 |

Chemotaxis towards stream (cell in Fig. 3)

| Cell location | Number of filopodia at each time point (seconds) | | | | | | | | | | | | | | |
|---|---|---|---|---|---|---|---|---|---|---|---|---|---|---|---|
| | 0 | 4 | 8 | 20 | 24 | 28 | 32 | 36 | 40 | 48 | 52 | 56 | 60 | 64 | 68 |
| Pseudopodium a | 3 | 4 | 3 | 3 | – | – | – | – | – | – | – | – | – | – | – |
| Pseudopodium b | 4 | 7 | 8 | 1 | 3 | 5 | 2 | 2 | 3 | 5 | 4 | 2 | 4 | 4 | 4 |
| Pseudopodium c | – | 2 | 3 | 7 | 5 | 7 | 6 | 5 | 6 | 5 | 3 | 6 | 3 | 3 | 3 |
| Cell body[a] | 1 | 1 | 1 | 0 | 3[a] | 3[a] | 3[a] | 2[a] | 2[a] | 2[a] | 1[a],1[b] | 1[a],1[b] | 1[a],1[b],1[c],2 | 1[a],1[b],1[c],2 | 1[a],1[b],1[c] |
| Uropod | 3 | 3 | 3 | 2 | 3 | 2 | 3 | 2 | 2 | 2 | 2 | 3 | 2 | 2 | 2 |
| Total | 11 | 17 | 18 | 13 | 14 | 17 | 14 | 11 | 13 | 14 | 11 | 13 | 14 | 14 | 12 |

Pseudopodial origins (a, c, d) of filopodia on the cell body are noted for the cell migrating in buffer in Fig. 2, pseudopodial origins (a, b, c) of filopodia on the cell body moving towards a stream in Fig. 3.

b were retracted, while a third pseudopod, c, formed (Fig. 2A). Between 24 and 36 seconds, pseudopod c became the new anterior end, expanding along the substratum and causing the cell to rotate in a counter clockwise direction. At 40 seconds, upon the complete retraction of pseudopod a, three filopodia originally formed on the pseudopod relocated to the cell body. Between 40 and 76 seconds, when pseudopod c extended along the substratum, a filopod that had formed on it was left behind on the cell body (starred at 56 seconds, Fig. 2A,B). Between 56 and 76 seconds, the cell extended a new lateral pseudopod (d) from its right flank, then between 76 and 108 seconds three additional pseudopodia, e, f and g (Fig. 2A). In Table 1, the locations of filopodia and the origins of those formed after 0 seconds are mapped through the 108 seconds of analysis. It is clear from this exercise that the majority of filopodia that formed anew during the 108 seconds of analysis, including those that appeared on the cell body, originated on pseudopodia (Table 1). Similar 4D analyses of filopod formation on four additional amoebae migrating in buffer supported the conclusions that the majority of filopodia originate in pseudopodia, and that the majority of filopodia on the main cell body form originally on pseudopodia and relocate to the cell body as a result of pseudopod retraction or extension.

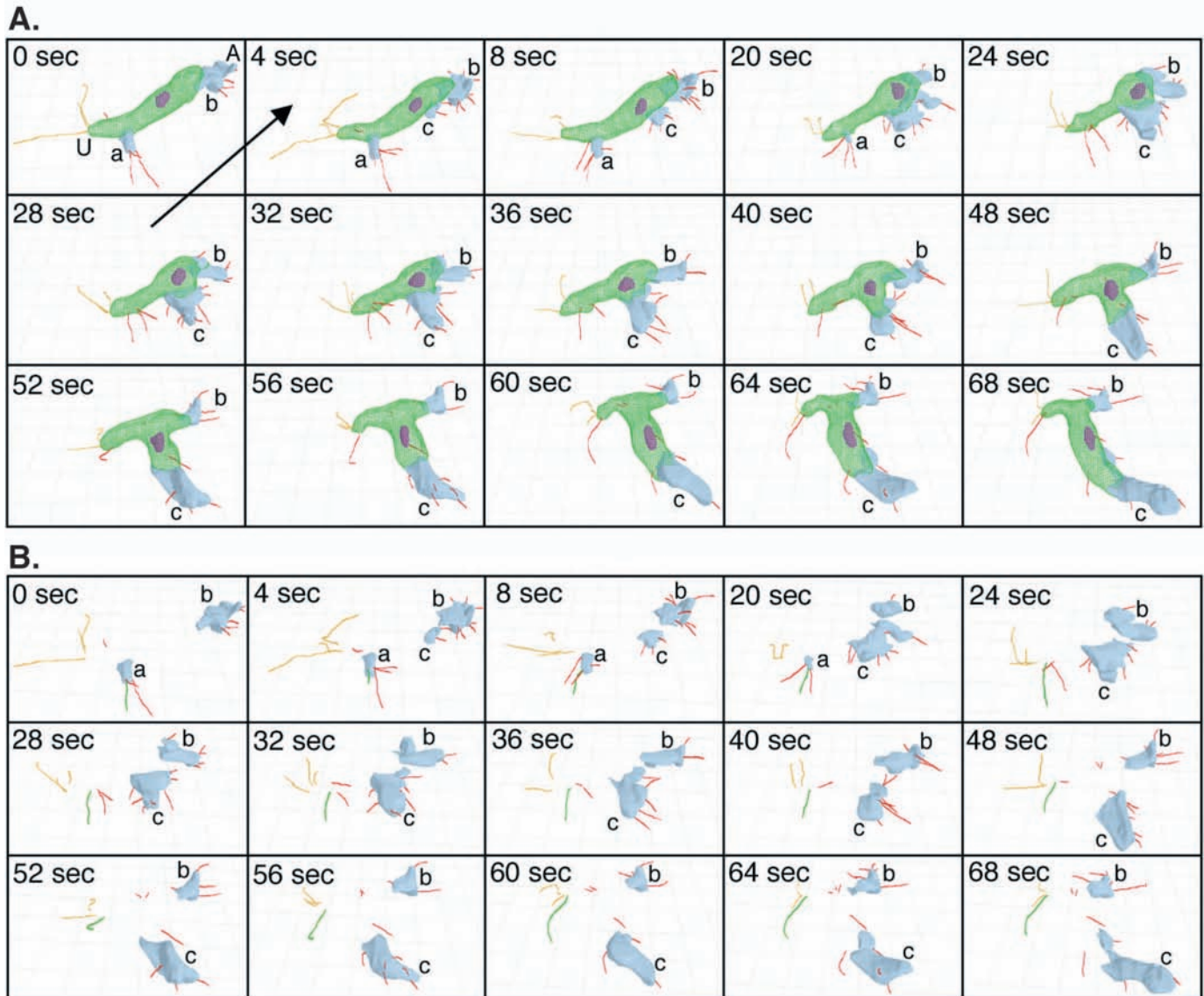### Filopod formation, retraction and relocation during chemotaxis

To assess filopod formation during chemotaxis, we analyzed individual cells that were turning towards multicellular streams late in the aggregation process. We selected this preparation as we were initially interested in determining whether cells that turn into a stream do so in response to physical contact of filopodia with the stream or to a spatial gradient of chemoattractant emanating from the stream. At 0 seconds, the anterior-posterior axis of the representative cell reconstructed in Fig. 3A paralleled the stream, which was out of view. As was the case for cells migrating in buffer, the majority of filopodia formed on pseudopodia, and the majority of filopodia on the cell body relocated there as a result of pseudopod retraction or extension (Fig. 3A,B; Table 1). The filopodia emanating from both pseudopodia and the cell body were relatively short and did not contact the stream. Different individuals scrutinized optical sections to be sure this was the case. Hence, the representative cell in Fig. 3, and four additional cells analyzed in a similar fashion (data not shown) turned into an adjacent stream by assessing a chemotactic signal emanating from the stream, not as a result of physical interactions between filopodia the and stream.

The representative cell in Fig. 3, and four additional cells analyzed in the same fashion (data not shown) turned into an adjacent stream by forming a lateral pseudopod towards the stream and turning into it. For each cell, the temporal and spatial dynamics of lateral pseudopod and filopodia could be separated into three phases, as will be demonstrated for pseudopod c in Fig. 4. The phases were of similar duration for the five analyzed cells.

### Phase one

In the first phase (0-20 seconds), pseudopod c grew from the right flank of the cell body, forming a blunt extension filled with non-particulate cytoplasm (Fig. 3A,B). The interface between the particulate cytoplasm of the main cell body and non-particulate cytoplasm of the pseudopod followed the contour of the cell body during phase one (i.e. particulate cytoplasm did not extend into the lateral protrusion) (Fig. 3A). A frontal view revealed that when pseudopod c was first visible (4 seconds), it extended off the substratum, but as it grew (8-20 seconds) it contacted and flattened on the substratum (Fig. 4). When pseudopod c first appeared at 4 seconds, it possessed

**Fig. 3.** Filopod formation, retraction and relocation for a representative cell turning towards an aggregation stream in response to a spatial gradient of chemoattractant. (A) Reconstruction of the full cell, including nucleus, pseudopodia and filopodia. (B) Reconstruction only of pseudopodia and filopodia. The cell is viewed from 55°. Time is presented in seconds (sec). The arrow in the lower right corner of the 0 second panel denotes the direction of the aggregation stream, which is out of sight beyond the lower right-hand corner. See legend to Fig. 1B for color code. A, anterior end of cell; U, uropod; a, b, c, pseudopodia in order of appearance.

two filopodia, and when it had finished growing at 20 seconds, it possessed six filopodia (Fig. 3A,B). When pseudopod c flattened on the substratum at 8 seconds, and through the next 12 seconds of growth, the majority of its filopodia also contacted the substratum (Fig. 4).

## Phase two

In the second phase (20-40 seconds), pseudopod c did not extend along the substratum or retract towards the stream, but it did continue to change shape (Fig. 3A,B). At 40 seconds, it transiently fragmented into two portions (Fig. 4). During phase two, the number of filopodia remained at roughly six per pseudopod (Fig. 5A). Through phase two, pseudopod c and its filopodia remained in contact with the substratum (Fig. 4).
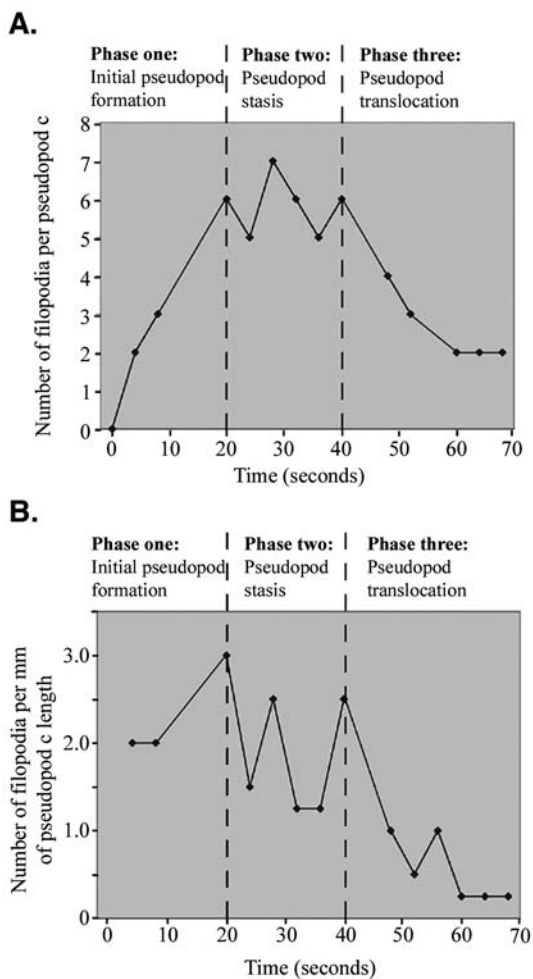
## Phase three

In the third phase (40-68 seconds), pseudopod c extended rapidly along the substratum towards the aggregation stream. Between 60 and 64 seconds, the apical end of the pseudopod lifted off the substratum (Fig. 4). As it extended towards the stream, the size of the pseudopodial zone containing non-particulate cytoplasm remained relatively constant (Fig. 3A,B). Hence, the interface between particulate and non-particulate cytoplasmic zone moved, or was drawn, in the direction of pseudopod translocation (Fig. 3A). Phase three therefore represents a committed turn, in which pseudopod c assumes the role of anterior end of the cell. During phase three, the total number of filopodia on pseudopod c decreased from approximately six to two, and the number of filopodia per $\mu$m along the proximal-distal axis of the pseudopod decreased from
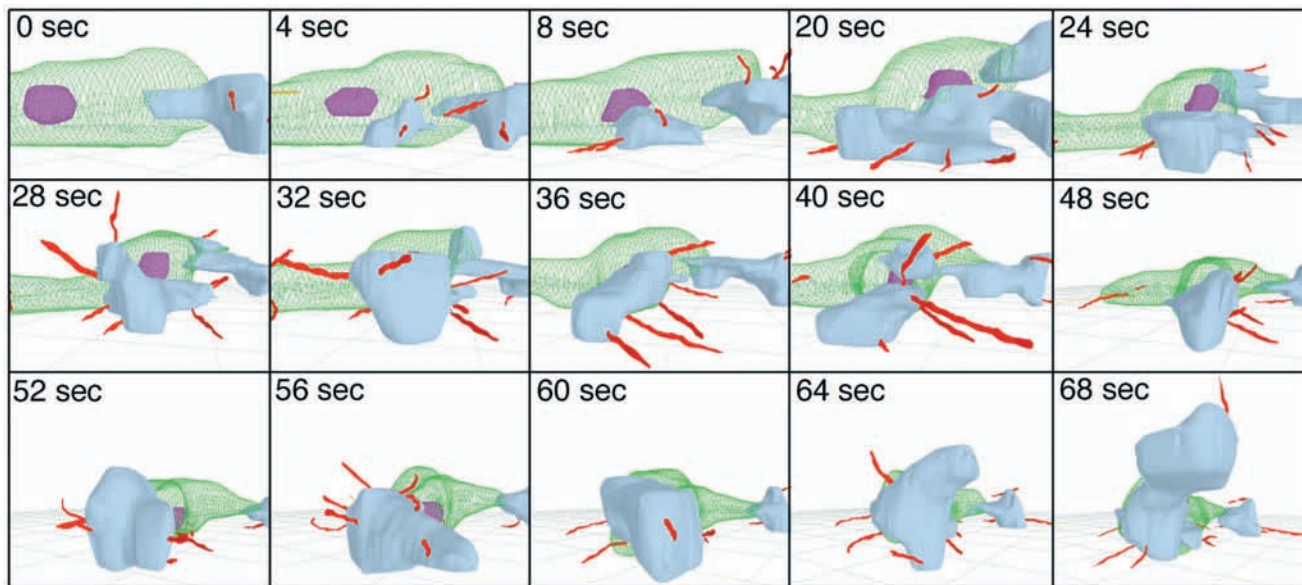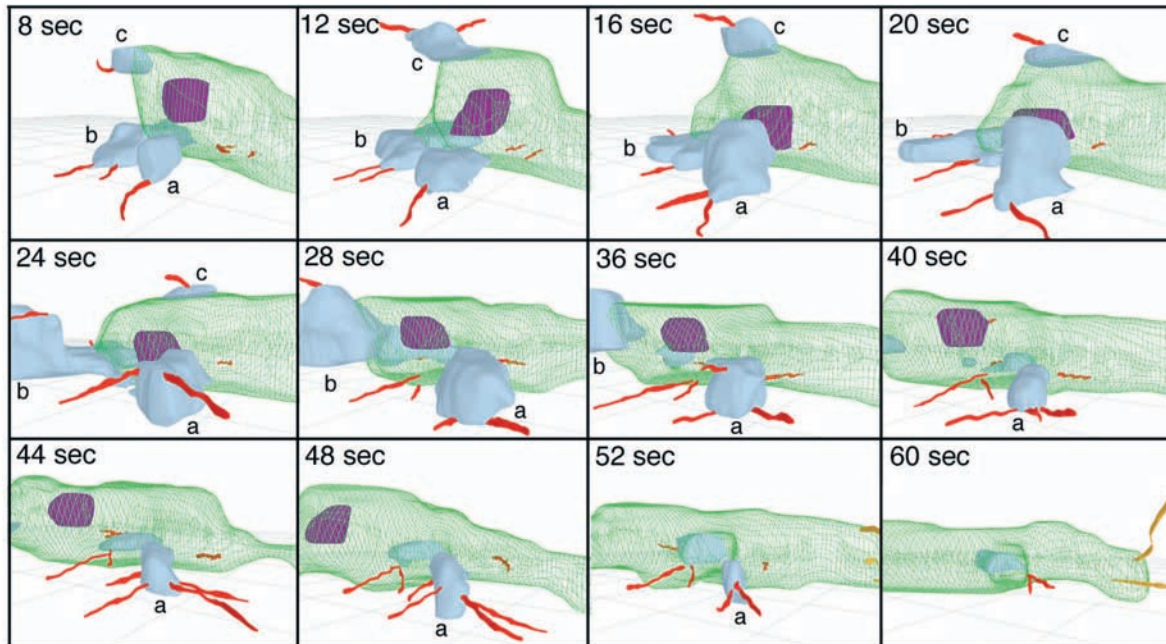
**Fig. 4.** Frontal view of the cell reconstructed in Fig. 3 reveals the interactions of pseudopod and filopodia with the substratum. Time is in seconds (sec). See legend to Fig. 1B for color code. Note the interaction between filopodia and substratum.

2.0 to 0.6 (Fig. 5A,B, respectively). The decrease in filopodia during phase three is evident in Fig. 3A,B.



**Fig. 5.** The density of filopodia changes during three discrete phases associated with pseudopod extension in response to a spatial gradient of chemoattractant emanating from an aggregation stream. In this case, filopodial number was monitored during extension of pseudopod c of the cell in Fig. 2. (A) Filopod number per pseudopod c. (B) Filopod number per μm of pseudopod c unit length. Pseudopodia of four additional cells turning towards a stream exhibited similar pseudopod and filopod dynamics. Note that filopodia are dense during phase two, but decrease in density in phase three.

Behavior in the three delineated phases suggests that a cell may make a decision, probably in the second phase, to either extend a lateral pseudopod and turn into it, or to retract it back into the cell body. In that putative decision-making phase, the majority of filopodia emanating from the pseudopod contact the substratum. If phase two indeed involves that decision, then when a pseudopod is formed in the wrong direction (i.e. away from the stream), it should undergo the first two phases in a manner similar to a pseudopod formed in the correct direction, but then retract. It was of interest to know the behavior of associated filopodia in retracting pseudopods. We, therefore, reconstructed pseudopodia formed at a 90° to 180° angle to the direction of the deduced chemotactic gradient (i.e. towards the stream). In Fig. 6, we have reconstructed a frontal view of a pseudopod that forms and then retracts, in this case pseudopod b of the cell reconstructed in Figs 3 and 4. This pseudopod had formed at a 90° angle to the deduced chemotactic gradient emanating from the stream. It grew to maximum size between 0 and 16 seconds (phase one), remained relatively constant between 16 and 36 seconds (phase two), and then was retracted back into the main cell body between 36 and 60 seconds (phase three) (Fig. 6). Clearly this pseudopod underwent an initial phase of pseudopod growth, then a second phase involving shape changes without growth, like a pseudopod that formed in the correct direction. However, in the third phase, the pseudopod

**Fig. 6.** Frontal view of a representative pseudopod that formed away from an aggregation stream and was retracted. Time is in seconds (sec). See legend to Fig. 1B for color code. This pseudopod, which formed between 0 and 16 seconds (phase one), maintained the same approximate volume between 16 and 28 seconds (phase two) and retracted between 36 and 60 seconds (phase three). Note the interactions between filopodia and substratum. a, b, c, pseudopodia.

was retracted, in marked contrast to a pseudopod that had formed in the correct direction. The majority of filopodia that extended from the pseudopod in phase two contacted the substratum, as was the case for pseudopodia formed in the correct direction. During pseudopod retraction, however, filopodia were retained and remained in contact with the substratum (Fig. 6), in contrast to the loss of filopodia during pseudopod extension in the correct direction. Similar filopodial dynamics were observed for three additional pseudopodia formed in the wrong direction by cells aligned with a stream.

### Chemoattractant regulates filopod formation

A comparison of the representative cell migrating in buffer in Fig. 2 and the cell responding to a spatial gradient of chemoattractant in Fig. 3 suggests that the latter possess more filopodia than the former. Indeed, the mean number of filopodia on cells in buffer (5.1±1.6; $n=24$) was less than half that in a spatial gradient of chemoattractant (11.2±3.1; $n=10$). Pseudopodia that formed in buffer did so in a more continuous fashion than those formed by cells in spatial gradients of chemoattractant, with little indication of three phases. These results suggest that filopod formation is regulated by the chemotactic receptor and are consistent with earlier reports that cells extend increased numbers of filopodia when treated with the chemoattractant cAMP (Kobilinsky et al., 1976; De Chastellier and Ryter, 1980; Choi and Siu, 1987) or, in the case of vegetative cells, folic acid (Rifkin and Isik, 1984). To analyze this response at the single cell level, cells were perfused in buffer for 5 minutes and then in buffer containing $10^{-6}$ M cAMP, the concentration of chemoattractant attained at the peak of the natural chemotactic wave (Tomchik and

Devreotes, 1981). This treatment results in a rapid receptor-mediated response within 25 seconds that has been demonstrated to include doubling of total F-actin, dismantling of F-actin enriched pseudopodia and a dramatic increase in F-actin and myosin II in the cell cortex, a dramatic reduction in the rate of cellular translocation, a dramatic decrease in cytoplasmic particle movement, rounding up of the cell body and blebbing from the cell surface (Hall et al., 1989; Wessels et al., 1989; Levi et al., 2002). After 2 minutes of perfusion with $10^{-6}$ M cAMP, cells partially adapt by reforming pseudopodia, but they remain relatively apolar, extend pseudopodia in random directions and do not translocate in a persistent fashion in any one direction (Wessels et al., 1989).

Within 25 seconds of addition of $10^{-6}$ M cAMP, cells dismantled pseudopodia, formed blebs around their periphery (color-coded purple) and retracted the great majority of their filopodia (Fig. 7A,B). After 4 minutes in $10^{-6}$ M cAMP, cells had partially adapted. They had stopped blebbing, extended pseudopodia again and reformed filopodia, remained relatively apolar and did not translocate in a persistent fashion (Fig. 7C). Although cells migrating in buffer possessed 5.1±1.6 ($n=24$) filopodia per cell, cells that had been treated with $10^{-6}$ M cAMP for 25 seconds possessed 0.3±1.0 ($n=20$) filopodia per cell, a 17-fold reduction. After 4 minutes in $10^{-6}$ M cAMP, cells had reformed filopodia, averaging 10±3 ($n=20$) per cell, twice the average number before treatment. Hence, the rapid addition of $10^{-6}$ M cAMP first caused filopod retraction, which occurred in parallel with the dismantling of pseudopodia and transient blebbing, and then overproduction of filopodia, which coincided with the reformation of pseudopodia. These results support the conclusion that filopodia formation is regulated by the chemotactic signal.
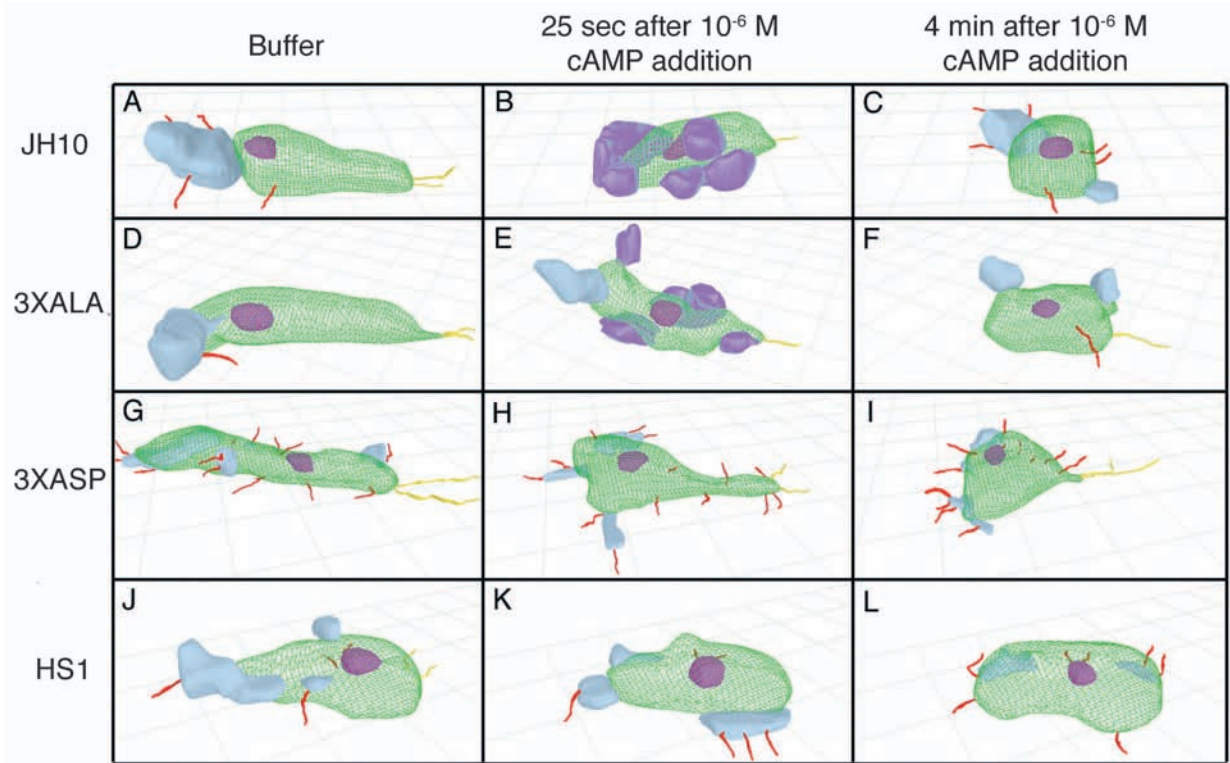
**Fig. 7.** The effects of the rapid addition of $10^{-6}$ M cAMP. $10^{-6}$ M cAMP was added to a representative control cell (A-C) and representative cells of the myosin II mutants 3XALA (D-F), 3XASP (G-I) and HS1 (J-L). Cells in perfusion chambers were first perfused with buffer alone for 5 minutes and then with buffer containing $10^{-6}$ M cAMP for 4 minutes. See legend to Fig. 2 for color code. Deep purple protrusions on the cell surface represent blebs.

## The stability of tail fibers

The posterior end (uropod) of polarized cells in buffer and in spatial gradients of chemoattractant possessed on average two tail fibers that were often much longer than the filopodia emanating from the rest of the cell body and pseudopodia (color-coded yellow, Figs 2 and 3). Tail fibers proved to be far more stable on average than those on the cell body and pseudopodia. They were replenished from filopodia that relocated from pseudopodia to the cell body (see filopod color-coded green in Fig. 3B). They were often retained when all other filopodia were retracted in response to the addition of $10^{-6}$ M cAMP (Fig. 7A,B). These results demonstrate that the stability of filopodia can differ as a function of location, but they do not distinguish between the possibility that filopodia that end up at the uropod are inherently more stable than others at the time of their inception and the possibility that the uropod provides a stabilizing environment.

## Myosin phosphorylation regulates filopod formation

It was recently demonstrated (Heid et al., 2004) that the phosphorylation-dephosphorylation of MHC plays a role in the stability of the anterior pseudopod, the regulation of lateral pseudopod formation, the efficiency of chemotaxis in a spatial gradient of cAMP and the capacity to enter aggregation streams. We, therefore, tested whether it played a role in filopod formation by analyzing the mutants, HS1, (Manstein et al., 1989), 3XALA, which contains mutant MHC that mimics the constitutively unphosphorylated state (Egelhoff et al., 1993; Egelhoff et al., 1996), and 3XASP, which contains mutant MHC that mimics the constitutively phosphorylated state (Egelhoff et al., 1993). We first compared the total number of filopodia on migrating control (JH10, HS1-rescue) and mutant cells perfused with buffer in the absence of chemoattractant. The mean number of filopodia per cell (±s.d.) for JH10, the control for HS1 and for the HS1-rescue, the control for 3XALA and 3XASP, was 5.1±1.6 and 5.2±0.9, respectively (Fig. 8A). The number per cell for the mutant HS1 was similar (5.1±3.3), but the s.d. was twice that of control cells, reflecting far greater variability, as is evident in the histogram in Fig. 8A. The number of filopodia per cell in the mutant 3XALA, however, was 1.2±1.1, approximately one-quarter that of control cells, whereas that of the mutant 3XASP was 11.0±3.4, more than twice that of control cells (Fig. 8A). An analysis of the number of filopodia per pseudopod revealed that the mean for 3XALA cells was significantly lower and the mean for 3XASP cells significantly higher than that for control cells (Fig. 8B). An analysis of lengths further revealed that filopodia that formed on 3XALA cells were significantly shorter than those of control cells HS1-rescue, 5.4±3.3 μm (*n*=22); 3XALA, 3.1±1.8 μm (*n*=23); *P*=0.002). These results were confirmed qualitatively in multiple clones of control and mutant strains.

When 3XALA cells were treated with $10^{-6}$ M cAMP, they became less polar, retracted the majority of filopodia and blebbed by 25 seconds (Fig. 7D,E), then extended new
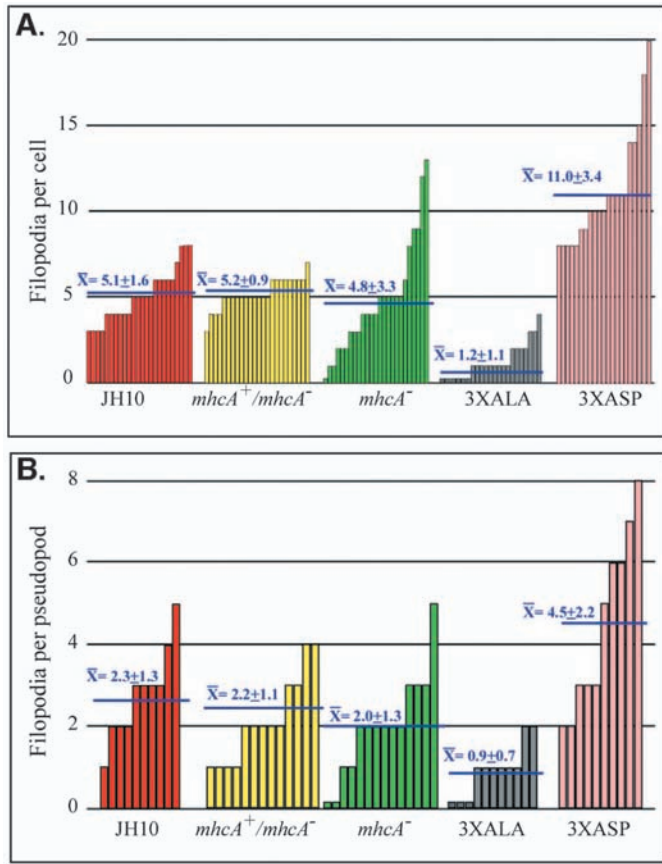
**Fig. 8.** Histograms of total number of filopodia. Number of filopodia, including tail fibers, per cell (A) and per pseudopod (B) for control and myosin mutant cells translocating in buffer. The mean±s.d. is presented above the histogram of each strain.

pseudopodia and reformed filopodia by 4 minutes (Fig. 7F), a response similar to that of control cells (Fig. 7A-C). 3XALA cells also produced more filopodia, on average, after the rebound (data not shown). However, when either 3XASP or HS1 cells were treated with $10^{-6}$ M cAMP, they neither retracted their filopodia nor blebbed after 25 seconds of treatment (Fig. 7G-L, respectively). There was no adaptive response and no increase in the number of filopodia after 4 minutes (data not shown). These results were confirmed qualitatively in additional clones of control and mutant cell lines. They demonstrate that the receptor-mediated response to the rapid addition of chemoattractant, which includes first the retraction and then overproduction of filopodia, requires unphosphorylated MHC.

## Discussion

Filopodia extend the surface of a cell into its environment. They increase surface area, increase the length of a cell, contact the surfaces of substrates, and interact with other cells and tissues. As they are bounded by the plasma membrane and form from the actin networks of pseudopodia (lamellipodia) (Svitkina et al., 2003), their actin filaments are contiguous with those in the cortex, and their cytoplasm is contiguous with that of the pseudopod and cell body. Hence, it has been suggested

that their function may be to sense the environment, either physically or chemotactically (Niell et al., 2004; Gallo and Letourneau, 2004; De Joussineau et al., 2003; Gerhart et al., 2003; Robles et al., 2003; Koleske, 2003; Lee and Goldstein, 2003; Dalby et al., 2004). To investigate their function(s), we have developed a computer-assisted system, DIAS 4.0, which allows us to reconstruct a living cell in 3D. It extends previous 3D DIAS software (Soll and Voss, 1998; Soll et al., 2000; Wessels et al., 1998; Heid et al., 2002) to include not only reconstruction of nucleus, pseudopodia and cell body, but also filopodia at intervals as short as two seconds, if desired. Here, we have used this technology for the first time to characterize the spatial and temporal dynamics of filopodia during migration and chemotaxis of *Dictyostelium* amoebae.

### The general characteristics of filopod formation

Our results demonstrate that for cells migrating in buffer or turning in a spatial gradient of chemoattractant late in the aggregation process, the majority of filopodia originate from pseudopodia, which is consistent with previous findings that filopodia arise from pre-existing F-actin networks (Small et al., 1998; Svitkina et al., 2003). A small minority of filopodia do originate on the cell body of *Dictyostelium*, but more commonly filopodia on the cell body originate on pseudopodia and relocate to the cell body through pseudopod retraction or extension. Our results also indicate that filopodia located on the uropod (tail fibers) are more stable and on average longer than filopodia located on pseudopodia and the rest of the cell body, and are replenished from filopodia that relocate from pseudopodia to the cell body. Different types of dendritic filopodia have been reported (Portera-Cailliau et al., 2003), supporting the view that filopodia on the same cell can exhibit different characteristics and hence, may serve different functions.

### Filopod dynamics and function during chemotaxis

Although filopodia formed during migration in buffer and in spatial gradients of chemoattractant exhibit similar general characteristics, the former have on average half the number of filopodia as the latter, supporting previous observations that the addition of chemoattractant to *Dictyostelium* causes an increase in filopodia (Kolilinsky et al., 1976; De Chastellier and Ryter, 1980; Choi and Siu, 1987; Rifkin and Isik, 1984). To characterize filopod dynamics during chemotaxis, we first analyzed cells turning towards multicellular aggregation streams through biased extension of a lateral pseudopod. Reconstructions of cells over time revealed that these turns were not mediated through physical contact of filopodia with cells in the stream, which appears to be the case when cells have entered the stream and are forming end-to-end contacts mediated by the adhesin gp80 (Choi and Siu, 1987). These biased turns were mediated, instead, through assessment of the chemotactic signal released by the multicellular aggregation stream, which we assume is in the form of a spatial gradient. We distinguished three phases of lateral pseudopod behavior associated with a biased turn toward a stream, each phase approximately 20 seconds in duration. In phase one, the lateral pseudopod evaginates and grows to a relatively blunt protrusion filled with non-particulate cytoplasm. At the end of

phase one, the pseudopod is in contact with the substratum. In phase two, the pseudopod continually changes shape, but does not extend towards the stream. Throughout phase two, the majority of filopodia remain in contact with the substratum. In phase three, the pseudopod expands towards the stream, drawing particulate cytoplasm into its proximal end. During lateral pseudopod extension in phase three, the number of filopodia on the pseudopod decreases dramatically. New filopodia that form on the extending pseudopod, do so transiently and do not contact the substratum. If a pseudopod forms on the flank of a cell away from a stream (i.e. in the wrong direction), it progresses through two behavioral phases similar to phase one and phase two of pseudopodia formed towards a stream (the right direction). However, in phase three, pseudopodia formed in the wrong direction are retracted back into the cell body. During retraction, a pseudopod retains its filopodia, which continue to contact the substratum. This is opposite the dynamics of filopodia on pseudopodia formed towards a stream. This sequence of behaviors suggests that during phase two, a cell decides whether it will extend the lateral pseudopod towards a stream or retract it. During this putative decision-making period, while the pseudopod continues to change shape, the majority of filopodia remain in contact with the substratum. When the decision is made to extend up the spatial gradient of chemoattractant, the number of filopodia on the pseudopod decreases dramatically, but when it makes a decision to retract, filopodia remain attached to the substratum. This sequence of events suggests that filopodia may play a role in repressing pseudopod extension and turning through interactions with the substratum.

The three phases displayed by lateral pseudopodia in chemotactic gradients rarely accompanied lateral pseudopod formation in buffer. Together with the observation that cells migrating in buffer possess on average half as many filopodia as cells undergoing chemotaxis, our results demonstrate that the natural chemotactic signal regulates filopod formation. Consistent with this suggestion, we found that the rapid addition of a high concentration of chemoattractant ($10^{-6}$ M cAMP) to cells in buffer, in addition to inducing the transient retraction of pseudopodia, blebbing and apolarity (Wessels et al., 1988), also induces transient retraction of almost all filopodia, followed by reformation of filopodia at twice their original density during adaptation.

## MHC phosphorylation-dephosphorylation regulates filopod formation

Both 3XALA cells, containing MHC that constitutively mimics the unphosphorylated state, and 3XASP cells, containing MHC that constitutively mimics the phosphorylated state, formed filopodia. However, although the former mutant possessed half as many filopodia, on average, as control cells, the latter possessed twice as many. Hence, the acts of phosphorylation or dephosphorylation of MHC are not essential for filopod formation. Rather, the state of MHC, which affects myosin II polymerization and the level of cortical tension, regulates the number of filopodia, suggesting that a balance of unphosphorylated and phosphorylated MHC in a cell must fine-tune the number of filopodia formed by pseudopodia. In addition, we show for the first time that unphosphorylated myosin is essential for the receptor-

mediated rapid response of *Dictyostelium* amoebae to cAMP, which includes the retraction of almost all filopodia followed by re-formation at twice the original number. Together, these results suggest that the formation and retraction of filopodia associated with chemotaxis may be regulated by receptor-mediated changes in the phosphorylation-dephosphorylation of MHC.

Interestingly, 3XASP cells, which formed more than twice as many filopodia as control or 3XALA cells, neither retracted filopodia nor formed blebs as did control and 3XALA cells in response to the rapid addition of $10^{-6}$ M cAMP. These results suggest that cells must have myosin II-mediated cortical tension in order to retract filopodia and bleb. The latter two events may in turn represent a dependent sequence. Blebs may arise as a result of excess plasma membrane resulting from the rapid retraction of the F-actin cores of filopodia. Consistent with these observations, a high-throughput screening assay identified the small molecule blebbistatin, which blocked non-muscle myosin II-dependent processes including blebbing (hence its name) in vertebrate cells, implicating myosin II function in the blebbing process (Straight et al., 2003).

## Other genes involved in filopod formation in *Dictyostelium*

Mutants of other genes implicated in the regulation of chemotaxis also exhibit defects in filopod formation. *Dictyostelium* null mutants of *VASP* exhibited a dramatic decease in filopod formation as well as a dramatic decrease in chemotactic efficiency (Han et al., 2002). Dd*vasp⁻* mutant cells were far less capable of maintaining pseudopodia on the substratum in a gradient of chemoattractant (Han et al., 2003), which is consistent with a role for filopodia in stabilizing pseudopodia on a surface. Furthermore, there is evidence that the Rac1 GTPases regulate filopodia (Dumantier et al., 2000). Expression of constitutively activated Rac1A resulted in a dominant-negative effect on filopod formation (i.e. no filopodia), whereas expression of constitutively inactivated Rac1A resulted in the formation of abnormally greater numbers of short filopodia. The former mutant exhibited both motility and development defects, consistent with a defect in chemotaxis. Mutants of two other genes have also been demonstrated to affect filopod formation. The *rasG⁻* mutant forms excess filopodia (Tuxworth et al., 1997), whereas transformation of wild-type cells with a constitutively activated form of RasG reduces the number of filopodia (Chen and Katz, 2000). Null mutants of two genes related to the mammalian phosphotidylinositide 3-kinases, *ddpik1⁻/ddpik2⁻*, also form excessive filopodia, although these mutants have been demonstrated to perform chemotaxis normally in a spatial gradient of cAMP (Buczynski et al., 1997). Myosin VII has also been found in filopodia (Tuxworth et al., 2001). It would appear that a number of different genes implicated in cell motility and chemotaxis play a role in the regulation of filopodia.

The results presented in this study demonstrate that filopodia originate on pseudopodia, are regulated by the chemotactic signal and appear to play a role in the decision by a cell to extend a lateral pseudopod and turn up a spatial gradient of chemoattractant. Their interactions with the substratum suggest that they play a role in stabilizing pseudopodia during

the decision-making phase of lateral pseudopod formation, although we have in no way excluded other potential roles. The filopod reconstruction software we describe here for the first time should aid in elucidating the exact role played by filopodia through future analyses of chemotaxis mutants.

## References

**Barsky, B. A.** (1988). Computer graphics and geometric modeling using beta-splines. pp. 1-9. Berlin: Springer-Verlag.

**Bear, J. E., Svitkina, T. M., Krause, M., Schafer, D. A., Loureiro, J. J., Strasser, G. A., Maly, I. V., Chaga, O. Y., Cooper, J. A., Borisy, G. G. et al.** (2002). Antagonism between Ena/VASP proteins and actin filament capping regulates fibroblast motility. *Cell* **109**, 509-521.

**Buczynski, G., Grove, B., Nomura, A., Kleve, M., Bush, J., Firtel, R. A. and Cardelli, J.** (1997). Inactivation of two *Dictyostelium discoideum* genes *DdPIK1* and *DdPIK2*, encoding proteins related to mammalian phosphatidylinositide 3-kinases, results in defects in endocytosis, lysosome to postlysosome transport, and actin cytoskeleton organization. *J. Cell Biol.* **136**, 1271-1286.

**Chen, C. F. and Katz, E. R.** (2000). Mediation of cell-substratum adhesion by RasG in *Dictyostelium*. *J. Cell Biochem.* **79**, 139-149.

**Choi, A. J. C. and Siu, C.-H.** (1987). Filopodia are enriched in a cell cohesion molecule of $M_r$ 80,000 and participate in cell-cell contact formation in *Dictyostelium discoideum*. *J. Cell Biol.* **104**, 1375-1387.

**Clark, E. R.** (1912). Further observations on living growing lymphatics: their relationship to the mesenchyme cells. *Am. J. Anat.* **13**, 351-379.

**Cocucci, S. and Sussman, M.** (1970). RNA is cytoplasmic and nuclear fractions of cellular slime mold amoebas. *J. Cell Biol.* **45**, 399-407.

**Cox, D., Ridsdale, A., Condeelis, J. and Hartwig, J.** (1995). Genetic deletion of ABP-120 alters the three dimensional organization of actin filaments in pseudopods. *J. Cell Biol.* **128**, 819-835.

**Dalby, M. J., Gadegaard, N., Riehle, M. O., Wilkinson, C. D. and Curtis, A. S.** (2004). Investigating filopodia sensing using arrays of defined nano-pits down to 35 nm diameter in size. *Int. J. Biochem. Cell Biol.* **36**, 2015-2025.

**De Chastellier, C. and Ryter, A.** (1980). Characteristic ultrastructural transformations upon starvation of *Dictyostelium discoideum* and their relationship with aggregation: study of wild type amoebae and aggregation mutants. *Biol. Cell.* **38**, 121-128.

**De Joussineau, C., Soule, J., Martin, M., Anguille, C., Montcourrier, P. and Alexandre, D.** (2003). Delta-promoted filopodia mediate long-range lateral inhibition in Drosophila. *Nature* **426**, 555-559.

**Dumontier, M., Höcht, P., Mintert, U. and Faix, J.** (2000). Rac1 GTPases control filopodia formation, cell motility, endocytosis, cytokinesis and development in *Dictyostelium*. *J. Cell Sci.* **113**, 2253-2265.

**Egelhoff, T. T., Lee, R. J. and Spudich, J. A.** (1993). *Dictyostelium* myosin heavy chain phosphorylation sites regulate myosin filament assembly and localization in vivo. *Cell* **75**, 363-371.

**Egelhoff, T. T., Nasmyth, T. V. and Brozovich, F. V.** (1996). Myosin-based cortical tension in *Dictyostelium* resolved into heavy and light chain-regulated components. *J. Muscle Res. Cell Motil.* **17**, 269-274.

**Falk, D. L., Wessels, D., Jenkins, L., Pham, T., Kuho, S., Titus, M. A. and Soll, D. R.** (2003). Shared, unique and redundant functions of three myosin Is (MyoA, MyoB and MyoF) in motility and chemotaxis in *Dictyostelium*. *J. Cell Sci.* **116**, 3985-3999.

**Gallo, G. and Letourneau, P. C.** (2004). Regulation of growth cone actin filaments by guidance cues. *J. Neurobiol.* **58**, 92-102.

**Gerhardt, H., Golding, M., Fruttiger, M., Ruhrberg, C. Lundkvist, A., Abramsson, A., Jeltsch, M., Mitcehll, C., Alitalo, K., Shima, D. and Betsholtz, C.** (2003). VEGF guides angiogenic sprouting utilizing endothelial tip cell filopodia. *J. Cell Biol.* **161**, 1163-1177.

**Hall, A. L., Warren, V., Dharmawardhane, S. and Condeelis, J.** (1989). Identification of actin nucleation activity and polymerization inhibitor in amoeboid cells: their regulation by chemotactic stimulation. *J. Cell Biol.* **109**, 2207-2213.

**Han, Y.-H., Chung, C. Y., Wessels, D. J., Stephens, S., Titus, M. A., Soll, D. R. and Firtel, R. A.** (2002). Requirement of a vasodilator-stimulated phosphoprotein family member for cell adhesion, the formation of filopodia, and chemotaxis in *Dictyostelium*. *J Biol. Chem.* **277**, 49877-49887.

**Hartwig, J. and Shevlin, P.** (1986). The architecture of actin filaments and the ultrastructural location of actin-binding protein in the periphery of lung macrophages. *J. Cell Biol.* **3**, 1007-1020.

**Heid, P., Voss, E. and Soll, D. R.** (2002). 3D-DIASemb: a computer-assisted system for reconstructing and motion analyzing in 4D every cell and nucleus in a developing embryo. *Develop. Biol.* **245**, 329-347.

**Heid, P. J., Wessels, D., Daniels, K. J., Zhang, H. and Soll, D. R.** (2004). The role of myosin heavy chain phosphorylation in *Dictyostelium* motility, chemotaxis and F-actin localization. *J. Cell Sci.* **117**, 1419-1435.

**Johnston, R. N., Atalar, A., Heiserman, S., Jipson, V. and Quate, C. F.** (1979). Acoustic microscopy: resolution of subcellular detail. *Proc. Natl. Acad. Sci. USA.* **76**, 3325-3329.

**Kobilinsky, L., Weinstein, B. I. and Beattie, D. S.** (1976). The induction of filopodia in the cellular slime mold *Dictyostelium discoideum* by cyclic adenosine monophosphate: mechanism of aggregation. *Dev. Biol.* **48**, 477-481.

**Koleske, A. J.** (2003). Do filopodia enable the growth cone to find its way? *Sci. STKE* **183**, 20.

**Lee, J. Y. and Goldstein, B.** (2003). Mechanisms of cell positioning during *C. elegans* gastrulation. *Development* **130**, 307-320.

**Levi, S., Polyakov, M. V. and Egelhoff, T. T.** (2002). Myosin II dynamics in *Dictyostelium*: determinants for filament assembly and translocation to the cell cortex during chemoattractant responses. *Cell Motil. Cytoskel.* **53**, 177-188.

**Lewis, A. K. and Bridgman, P. C.** (1992). Nerve growth cone lamellipodia contain two populations of actin filaments that differ in organization and polarity. *J. Cell Biol.* **119**, 1219-1243.

**Mallavarapu, A. and Mitchison, T.** (1999). Regulated actin cytoskeleton assembly at fiolpodium tips controls their extension and retraction. *J. Cell Biol.* **146**, 1097-1106.

**Manstein, D. J., Titus, M. A., DeLozanne, A. and Spudich, J. A.** (1989). Gene replacement in *Dictyostelium*: generation of myosin null mutants. *EMBO J.* **8**, 923-932.

**Mejillano, M. R., Kojima, S-i., Applewhite, D. A., Gertler, F. B., Svitkina, T. M. and Borisy, G. G.** (2004). Lamellipodial versus filopodia mode of the actin nanomachinery: pivotal role of the filament barbed end. *Cell* **118**, 363-373.

**Niell, C. M., Meyer, M. P. and Smith, S. J.** (2004). *In vivo* imaging of synapse formation on a growing dendritic arbor. *Nat. Neurosci.* **7**, 254-260.

**Portera-Cailliau, C., Pan, D. T. and Yuste, R.** (2003). Activity-regulated dynamic behavior of early dendritic protrusions: evidence for different types of dendritic filopodia. *J. Neurosci.* **23**, 7129-7142.

**Rifkin, S. L. and Isik, F.** (1984). Effects of folic acid upon filopodia of *Dictyostelium discoideum* vegetative cells. *Cell Motil. Cytoskel.* **4**, 129-135.

**Robles, E.**, **Huttenlocher, A. and Gomez, T. M.** (2003). Filopodial calcium transients regulate growth cone motility and guidance through local activation of calpain. *Neuron* **38**, 597-609.

**Salas-Vidal, E. and Lomeli, H.** (2004). Imaging filopodia dynamics in the mouse blastocyst. *Dev. Biol.* **265**, 75-89.

**Sato, K., Hattori, S., Irie, S. and Kawashima, S.** (2003). Spike formation by fibroblasts adhering to fibrillar collagen I gel. *Cell Struct. Func.* **28**, 229-241.

**Small, J. V.** (1988). The actin cytoskeleton. *Electron Microsc. Rev.* **1**, 155-174.

**Small, J. V.** (1994). Lammellipodia architecture: actin filament turnover and the lateral flow of actin filaments during motility. *Semin. Cell Biol.* **5**, 157-163.

**Small, J. V., Rottner, K., Kaverina, I. and Anderson, K. I.** (1998). Assembling an actin cytoskeleton for cell attachment and movement. *Biochim. Biophys. Acta.* **1404**, 271-481.

**Small, J. V., Stradal, T., Vignal, E. and Rottner, K.** (2002). The lamellipodium: where motility begins. *Trends Cell Biol.* **12**, 112-120.

**Soll, D. R.** (1979). Timers in developing systems. *Science* **203**, 841-849.

**Soll, D. R.** (1995). The use of computers in understanding how animal cells crawl. *Int. Rev. Cytol.* **163**, 43-104.

**Soll, D. R. and Voss, E.** (1998). *Two and three dimensional computer systems for analyzing how cells crawl*. In *Motion Analysis of Living Cells* (eds D. R. Soll and D. Wessels), pp. 25-52. New York: John Wiley.

**Soll, D. R., Voss, E., Johnson, O. and Wessels, D. J.** (2000). Three-dimensional reconstruction and motion analysis of living crawling cells. *Scanning* **22**, 249-257.

**Soll, D. R., Wessels, D., Zhang, H. and Heid, P.** (2002). A contextual framework for interpreting the roles of proteins in motility and chemotaxis in *Dictyostelium discoideum*. *J. Musc. Res. Cell Motil*. **23**, 659-672.

**Stites, J., Wessels, D., Uhl, A., Egelhoff, T. E., Shutt, D. and Soll, D. R.** (1998). Phosphorylation of the *Dictyostelium* myosin II heavy chain is necessary for maintaining cellular polarity and suppressing turning during chemotaxis. *Cell Motil. Cytoskel*. **39**, 31-51.

**Straight, A. F., Cheung, A., Limouze, J., Chen, I., Westwood, N. J., Sellers, J. R. and Mitchison, T. J.** (2003). Dissecting temporal and spatial control of cytokinesis with a myosin II inhibitor. *Science* **299**, 1743-1747.

**Sussman, M.** (1987). *Cultivation and synchronous morphogenesis of Dictyostelium under controlled experimental conditions*. In *Methods in Cell Biology*. Vol. 28 (ed. J. A. Spudich) pp. 9-29. Orlando: Academic Press.

**Svitkina, T. M. and Borisy, G. G.** (1999). Progress in protrusion: the tell-tale scar. *Trends Biochem. Sci*. **24**, 432-436.

**Svitkina, T. M., Bulanova, E. A., Chaga, O. Y., Vignjevic, D. M., Kojima, S.-I., Vasiliev, J. M. and Borisy, G. G.** (2003). Mechanism of filopodia initiation by reorganization of a dendritic network. *J. Cell Biol*. **160**, 409-421.

**Tokuo, H. and Ikebe, M.** (2004). Myosin X transports Mena/VASP to the tip of filopodia. *Biochem. Biophys. Res. Commun*. **319**, 214-220.

**Tomchik, S. J. and Devreotes, P. N.** (1981). cAMP waves in *Dictyostelium discoideum*: Demonstration by an isotope dilution fluorgraphic technique. *Science* **212**, 443-446.

**Tuxworth, R. I., Cheetham, J. L., Machesky, L. M., Spiegelmann, G. B., Weeks, G. and Insall, R. H.** (1997). *Dictyostelium* RasG is required for normal motility and cytokinesis, but not growth. *J. Cell Biol*. **138**, 605-614.

**Tuxworth, R. I., Weber, I., Wessels, D., Addicks, G. C., Soll, D. R., Gerisch, G. and Titus, M. A.** (2001). A role for myosin VII in dynamic cell adhesion. *Curr. Biol*. **11**, 318-329.

**Varnum, B., Edwards, K. and Soll, D. R.** (1986). The developmental regulation of single cell motility in *Dictyostelium discoideum*. *Dev. Biol*. **113**, 218-227.

**Wessels, D., Schroeder, N., Voss, E., Hall, A., Condeelis, J. and Soll, D. R.** (1989). cAMP mediated inhibition of intracellular particle movement and actin reorganization in *Dictyostelium*. *J. Cell Biol*. **109**, 2841-2851.

**Wessels, D., Murray, J. and Soll, D. R.** (1992). The complex behavior cycle of chemotaxing *Dictyostelium* amoebae is regulated primarily by the temporal dynamics of the natural wave. *Cell Motil. Cytoskel*. **23**, 145-156.

**Wessels, D., Voss, E., von Bergen, N., Burns, R., Stites, J. and Soll, D. R.** (1998). A computer-assisted system for reconstructing and interpreting the dynamic three-dimensional relationships of the outer surface, nucleus and pseudopodia of crawling cells. *Cell Motil. Cytoskel*. **41**, 225-246.

**Zhang, H., Wessels, D., Fey, P., Daniels, K., Chisholm, R. and Soll, D. R.** (2002). Phosphorylation of the myosin regulatory light chain plays a role in cell motility and polarity during *Dictyostelium* chemotaxis. *J. Cell Sci*. **115**, 1733-1747.